CHINESE OPTICS LETTERS

Vol. 22, No. 3 | March 2024

Research progress of integrated optical gyroscope

Hongjie Guo (郭宏杰)[1,2], Haifeng Liu (刘海锋)[1,3*], Ming Lei (雷 明)[4], Manqing Tan (谭满清)[1], and Zhigang Song (宋志刚)[1]

[1] Institute of Semiconductors, Chinese Academy of Sciences, Beijing 100083, China

[2] College of Materials Science and Opto-electronics Technology, University of Chinese Academy of Sciences, Beijing 100049, China

[3] Beijing Huairou Instruments and Sensors Co., Ltd., Beijing 101400, China

[4] Beijing Institute of Automation and Control Equipment, Key Laboratory of National Defense Science and Technology of Inertial Technology, Beijing 100074, China

*Corresponding author: liuhaifeng@semi.ac.cn

Received June 16, 2023 | Accepted October 27, 2023 | Posted Online March 15, 2024

Integrated optical gyroscopes (IOGs) have been an efficient tool for numerous applications in various fields, including inertial navigation, flight control, and earthquake monitoring. Here, we review the progress of integrated optical gyroscopes based on two categories of integrated interferometric optical gyroscopes (IIOGs) and integrated resonant optical gyroscopes (IROGs).

Keywords: integrated optical gyroscopes; interferometric optical gyroscopes; integrated resonant optical gyroscopes.
DOI: 10.3788/COL202422.031302

1. Introduction

The optical gyroscope is a device that uses the principle of optics to measure angular velocity and direction. It consists of a rotating rotor and a pair of optoelectronic detectors, which can measure the rotation of an object by detecting changes in the light path. Optical gyroscopes are widely used in inertial navigation, flight control, earthquake monitoring, and other fields[1]. Optical gyroscopes use the Sagnac effect, which is a well-known phenomenon in optical physics. When a beam of light splits into two beams and travels around a loop in opposite directions, the time it takes for the two beams to travel around the loop will be different if the loop is rotating[2]. This is because the rotation of the loop causes a phase shift between the two beams, which results in an interference pattern that is proportional to the rotation rate of the loop.

In recent years, advances in photonic integrated circuits (PICs) have led to the development of novel devices such as on-chip lasers, photonic integrated circuits, and optoelectronic neural networks[3]. These devices have the potential to revolutionize fields such as computing, sensing, and communications. One of the key advantages of the integrated optical gyroscope is the ability to combine multiple functions onto a single chip, leading to improved performance and reduced size, weight, and power consumption, making it suitable for a wider range of applications[4].

Here, we classify integrated optical gyroscopes (IOGs) into two categories, including integrated interferometric optical gyroscopes (IIOGs) and integrated resonant optical gyroscopes (IROGs)[5]. In IIOGs, the interferometric fiber optic gyroscope (IFOG) is a commonly used technology that has potential for further integration. In this regard, three integration routes have been analyzed based on the IIOG's technology, namely, hybrid integration, multifunction integrated optic circuits (MIOCs), and coiled waveguides. In IROGs, the material platform for the integrated resonant gyroscopes and the optical structure design of the resonant microcavities have been studied.

2. Integrated Interferometric Optical Gyroscopes

The configuration of interferometric optical gyroscopes, shown in Fig. 1, involves the use of a 50/50 coupler[6,7] (3 dB coupler) to divide light from the source into clockwise (CW) and counterclockwise (CCW) beams within a waveguide coil or fiber coil. When the gyroscope rotates perpendicularly to its plane, the counter-propagating beams experience distinct phase shifts that are directly proportional to the velocity of the rotation. These phase shifts are then converted to intensity information and detected by a photodetector (PD). To achieve optimal sensitive operation bias for the gyroscope, a phase modulator (PM) is employed, which is an essential component of the interferometric gyroscope's system. Additionally, coupler-I is used to separate the input and output beams, while the polarizer filters out the TM mode to enhance the precision of the fiber optic gyroscope.

The realization of integrated interferometric optical gyroscopes primarily involves two main approaches: the development of hybrid integration and the use of integrated waveguide coils. Hybrid integration is a crucial factor in

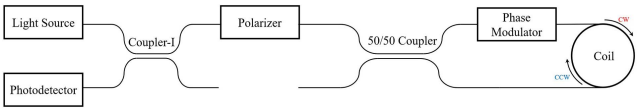

Fig. 1. Configuration of interferometric optical gyroscopes.

achieving high accuracy and small size simultaneously. This involves integrating multiple devices, such as light sources, photodetectors, couplers, polarizers, and phase modulators, onto a single chip through semiconductor and waveguide processing technologies. By doing so, IIOGs can operate with increased precision while maintaining a compact form factor. The integrated waveguide coils serve as sensing modules to accumulate the Sagnac phase shift, which is usually based on different material platforms such as silicon-on-insulator (SOI), silicon nitride (SiN), and silica.

2.1. Hybrid integration

The integration of passive devices such as couplers on a single material platform, followed by the bonding of light sources, photodetectors, and phase modulators onto a chip, is a common solution for mixed-integration in IIOGs. The most popular platforms for IIOGs are silica, silicon, and lithium niobate.

The silica platform has attained a high degree of maturity, making it the most well-established platform currently available. In addition to this, commercialization of silicon oxide-based IIOGs has been successfully accomplished. In 2019, Wang *et al.* proposed a low-cost, high-end, tactical-grade fiber optic gyroscope based on a photonic integrated circuit (PIC)[8], as shown in Fig. 2(b). The PIC FOG has an optimized waveguide

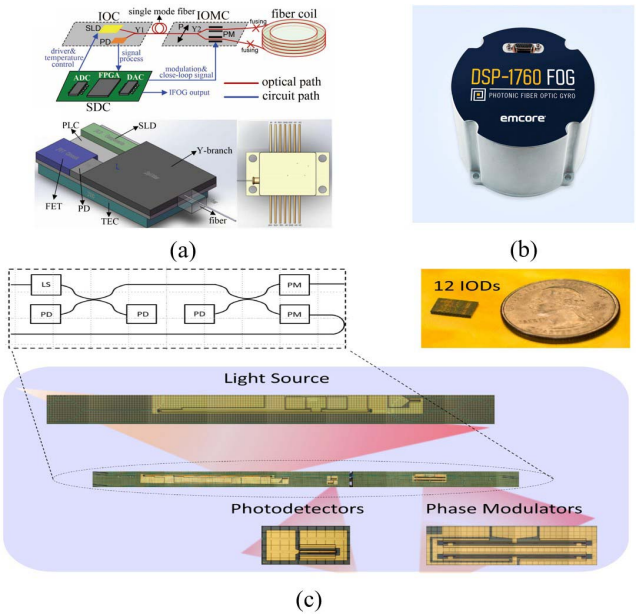

Fig. 2. (a) IIOGs based on the silica platform from Shang *et al.*[9]. (b) IIOGs based on the silica platform from Wang *et al.*[8]. (c) IIOGs based on the silicon platform from Tran *et al.*[12].

component and a circuit design that effectively minimize errors from the polarization cross-coupling, the parasitic Michelson interferometer, and back-scattered light. The resulting photonic gyro has demonstrated excellent performance with a low angular random walk (0.59 deg $/\sqrt{\text{h}}$), bias drift (0.048 deg/h), and instability over a wide temperature range. In 2020, Shang *et al.*[9] put forth a proposal for an interferometric fiber optic gyroscope (IFOG) capable of near-navigation-grade accuracy, as shown in Fig. 2(a). The IFOG is based on an integrated optical chip that contains a light source, a photodiode, and a 50/50 coupler, all within a compact area of 48 mm^2. When coupled with a 500-m-long fiber coil having a diameter of 4.5 cm, the integrated IFOG exhibited an angular random walk (ARW) of approximately 0.014 deg $/\sqrt{\text{h}}$ and a bias instability of about 0.018 deg/h. These results indicate that the proposed IFOG has the potential to achieve high-precision navigation applications. In 2022, Suo *et al.*[10] proposed a novel IIOG that employs a specially designed photo-electronic chip and a mini polarization maintaining photonic-crystal fiber (PM-PCF) coil. The use of a 600-m-long ultra-thin diameter PM-PCF coil with an outer diameter of about 26 mm results in a high accuracy IFOG with a bias stability of 0.05 deg/h at the integration time of 100 s, an ARW of 0.0083 deg $/\sqrt{\text{h}}$ at room temperature, and a bias stability of 0.11 deg/h over a wide temperature range.

The silicon platform[11] is considered the most promising platform due to its compatibility with complementary metal-oxide-semiconductor (CMOS) technology, which enables the realization of true IIOGs. In 2017, Tran *et al.*[12] proposed a novel solution for the integration of various components in an integrated optical driver (IOD) aimed at improving the performance of IIOGs. The IOD chip [shown in Fig. 2(c)] features a Fabry–Perot multi-mode laser, photodiodes, phase modulators, and adiabatic 3-dB splitters, all within a 0.5 mm × 9 mm area, representing a significant advancement in the field. This research demonstrates the first working IIOG driven by a fully integrated chip. However, more characterizations on packaged devices are necessary to fully evaluate the IOD-driven-gyroscope, particularly with regard to noise characteristics and limitations. In 2020, Wang *et al.*[13] presented a novel IIOG based on a silicon photonics platform. The compact design of the device incorporates all the necessary passive and active components, except for the light source and coil which are external. Notably, the findings of the Allan deviation analysis revealed an ARW of 0.093 deg $/\sqrt{\text{h}}$ and a bias instability of less than 0.6 deg/h, indicating high precision performance of the IIOG. It is worth noting that this work presents the first successful demonstration of a miniaturized Si-based IIOG that is deemed suitable for tactical applications.

In the field of lithium niobate material platforms, the multifunction integrated optic circuit (MIOC) is a commonly used structure, comprising a polarizer, a 50/50 coupler, and a phase modulator, as shown in Fig. 3(a)[14]. The performance of an MIOC-based IIOG is largely dependent on key parameters, such as modulation efficiency ($V_\pi L$), polarization extinction ratio (PER), and loss. Therefore, optimizing these parameters is

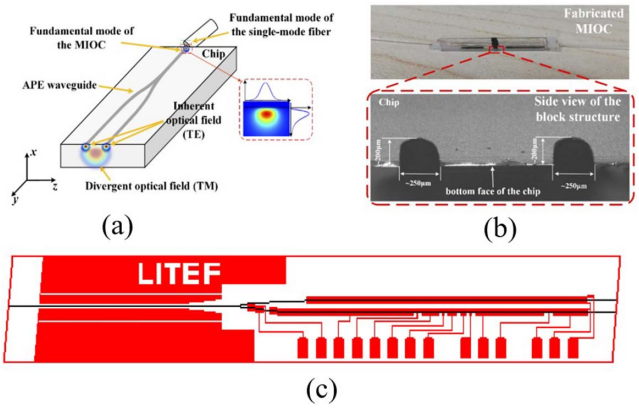

Fig. 3. (a) Schematic diagram of the MIOC[16]. (b) Optimized block structure for the MIOC to improve the PER[16]. (c) Schematic diagram of a mixed-signal MIOC[15].

crucial in achieving high-performance IIOGs. In 2017, Deppe *et al.*[15] proposed a mixed-signal MIOC that integrates a 12-bit digital-to-analog converter (DAC) through binary-weight divided electrodes for electro-optical phase modulation, and an additional small electro-optical phase shifter, as shown in Fig. 3(c). The advantages of this structure include the ability to drive the electrodes from the digital ASIC with no need for an additional DAC. The mixed-signal MIOC provides a new direction for the development of IIOGs. In 2021, Liu *et al.* of Beihang University[16] proposed an optimized block structure for the MIOC, as shown in Fig. 3(b). The structure consists of double absorption trenches located at the bottom of the MIOC. Compared to traditional designs, the optimized MIOC has an average PER value exceeding 75 dB. This approach has great potential for reducing polarization nonreciprocal errors in high-precision FOG applications.

In recent times, the field of electro-optic modulators has witnessed significant advancements due to the emergence of thin-film lithium niobate (TFLN) as a promising platform. This is attributed to its distinguishing features, such as low optical loss, high modulation efficiency, and ultrafast modulation ($V_\pi L$<1.5 V·cm). In 2022, Guo *et al.*[17] proposed a novel MIOC design that employed a vertical electrode structure based on a TFLN platform. The study provided valuable insights into the realization of compact footprint and high-performance in MIOC. In addition to MIOC, other researchers have proposed the use of a double Y-junction in integrated optical chips (IOCs). In 2022, Shang *et al.*[18] presented an IOC that integrates a light source, a photodiode, a polarizer, a double Y-junction, and a phase modulator. By utilizing a small-diameter sensing coil and a signal-detection circuit, an IIOG based on IOC technology was realized with a bias instability of 0.12 deg/h over 1000 min.

In addition to the above three common material platforms, there are proposals for IIOGs based on GaAs[19] and InP[20] platforms. Research on these platforms is limited. Overall, heterogeneous integration technology can greatly reduce the size, weight, cost, and power consumption of IIOGs while also improving sensitivity. Currently, the silica platform is the most commercially viable and mature, whereas the Si platform shows promise as the most ideal platform for the future. However, before TFLN can become the primary technology route for high-precision IIOGs, certain issues, such as high coupling loss and low polarization extinction ratio (PER), must be addressed. Once these problems are resolved, TFLN may become the main technological route for high-precision IIOGs.

2.2. Integrated waveguide coils

IIOGs utilize long coiled waveguides as sensing modules to accumulate the Sagnac phase shift. However, achieving high responsivities in chip-scale IIOGs is more challenging compared to fiber IOGs because the responsivity of the IOG is proportional to its area. Figure 4 shows a typical integrated IOG that has been implemented using various material platforms, including SOI[21], silica[22], and SiN[23,24].

An IIOG with an SOI multi-mode coiled waveguide with a small footprint of 600 μm × 700 μm has been demonstrated[25], achieving a gyroscope sensitivity of 51.3 deg/s. The coiled waveguide had a length of 2.76 cm with 15 crossings, an average propagation loss of 1.328 dB/cm, and an average crossing loss of 0.075 dB at 1550 nm. In a subsequent study, the same team proposed an on-chip silicon mode-assisted IIOG using different modes propagating oppositely in a waveguide coil based SOI[21], which avoids integrating the polarization-maintaining fiber and circulator [Fig. 4(a)]. The simulation results indicate a detectable angular rate of 0.64 deg/s with a small footprint of 3.85×10^{-3} m^2.

The use of SiO_2 coiled waveguides has been explored in IIOGs, as shown in Fig. 4(b). In this approach[22], the coiled waveguide is connected to other optical components in the gyroscope system through fiber-tail coupling. The insertion loss of the fabricated coiled waveguide, which had 11 crossings, was minimized by optimizing the bend radius and the space between the adjacent loops, resulting in a low insertion loss of 8.37 dB. The resulting IOG exhibited a low bias drift of 7.32 deg/h and

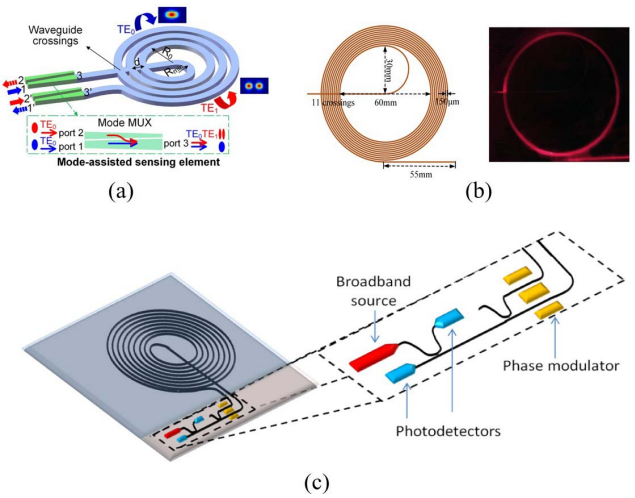

Fig. 4. Schematic diagram of the integrated waveguide coils. (a) SOI[21], (b) SiO_2[22], (c) SiN[23].

Table 1. Performance of the Integrated Coil Waveguides.

Platform	Insertion Loss	Length	Footprint	ARW	Bias Drift
SOI[21]		29 mm	0.42 mm^2		51.3 deg/h
SiO_2[22]	8.37 dB	2.14 m	121 cm^2	1.26 deg $/\sqrt{h}$	7.32 deg/h
SiN[23]	16.2 dB	3 m	12.57 cm^2	8.52 deg $/\sqrt{h}$	58.7 deg/h

a low ARW of 1.26 deg $/\sqrt{h}$, demonstrating the effectiveness of this approach. An IIOG with a SiN[24] coiled waveguide [Fig. 4(c)] achieved a detection limit of 19 deg $/(h \cdot \sqrt{Hz})$ in an area smaller than 10 cm^2. Additionally, a commercial-grade IIOG was demonstrated based on a 3-m-long large-area SiN sensing coil, with an ARW and bias drift of 8.52 deg $/\sqrt{h}$ and 58.7 deg /h, respectively.

The aforementioned studies showcase the efficacy of various techniques in developing highly sensitive and compact IIOGs utilizing integrated coil waveguides. To comprehensively overview the current state-of-the-art in integrated coil waveguides, Table 1 has been compiled to summarize and compare the performance of these waveguides. From Table 1, we can observe that there are two factors that limit the performance of IIOGs. First, the length of the integrated waveguide coil is too short, and the multi-layer stacking technology is not mature enough, which makes it difficult to achieve the theoretically high accuracy. Second, the unit transmission loss is too large, making it challenging to achieve the minimum total loss within a certain length.

3. Integrated Resonant Optical Gyroscopes

The IOG measures the phase difference between clockwise and counterclockwise light paths, while the ROGs measure the frequency difference between the two directions of light in an optical resonant cavity. The sensitivity of the ROG depends on its ability to detect the frequency difference, which can be improved by increasing the time that light spends in the resonant cavity or by enhancing the Sagnac effect. In this section, we focus on the current research progress of both approaches in the field of IROGs.

3.1. Resonant microcavity platform

The high-quality factor (Q) of a resonant cavity characterizes the degree of confinement of the cavity to the optical field on a temporal scale. A high Q value corresponds to a narrow linewidth and a low loss of the resonant cavity mode, indicating a longer lifetime of photons inside the cavity. Therefore, achieving a high Q value optical microcavity is essential for realizing high-performance IROGs. The preparation of the resonant cavity's materials and structures influences the Q value with commonly used materials, including SiO_2[26–30], SOI, CaF_2, polymer and SIN[31–33], and popular resonant cavity structures, including the optical waveguide ring resonator (WRR) and the whispering-gallery mode resonator (WGMR). The research progress on optical resonant cavities is presented in Table 2.

SiO_2 is a commonly used material for IROGs due to its low transmission loss. Compared to the WRR, the WGMR [as shown in Fig. 5(a)] can achieve higher Q for smaller volumes, but the increased complexity in its fabrication is a notable challenge. Silicon nitride (SiN) is also utilized in IROGs, owing to its high polarization extinction ratio, as shown in Fig. 5(b), which helps reduce polarization noise. Electro-optic (EO) polymers[34,40] [Fig. 5(c)] are a promising alternative due to their high electro-optic coefficients, which can improve the modulation efficiency and overall performance of IROGs. In addition, long-range surface plasmon-polariton-doped[35,41] gain media can compensate for the propagation loss while reducing the pump noise compared to conventional optical waveguides,

Table 2. Research Progress of the Optical Resonant Cavities.

Material	Year	Research Team	Diameter (cm)	Q (10^6)	Loss
SiO_2[30]	2017	Zhejiang University	2.5	14.6	
SiO_2[26]	2013	NIST	0.28	290	
SIN[31]	2022	Beihang University	3.5	15.4	1.2 dB/m
SIN[32]	2021	Beihang University	1.6		2.64 dB/m
Polymer[34]	2022	Southeast University	2	1	0.118 dB/cm
LRSPP[35]	2014	Southeast University	4		0.14 dB/cm
InP[36]	2013	Politecnico di Bari	2.6	0.97	0.45 dB/cm
CaF_2[37]	2007	California Institute of Technology		100,000	
CaF_2[38]	2017	Eowaves	0.7	> 100	
SOI[39]	2012	Massachusetts Institute of Technology	0.49	220	2.7 dB/m

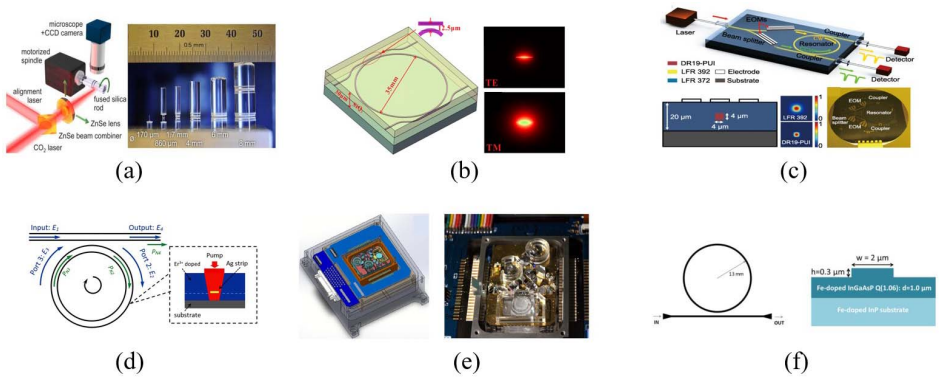

Fig. 5. Schematic diagram of the resonant microcavity platform. (a) SiO_2[26], (b) SiN[31], (c) polymer[34], (d) LRSPP[35], (e) CaF_2[38], and (f) InP[36].

which is shown in Fig. 5(d). Furthermore, the long-range surface plasmon-polariton (LRSPP) only transmits transverse magnetic (TM) mode polarized light, thus avoiding polarization crosstalk noise. Calcium fluoride (CaF_2)[37,38] crystal [Fig. 5(e)] is another unique material with a high refractive index that can be used to fabricate WRR and WGMR with ultra-high Q, making them commercially viable. InP[36] and SOI[39,42] represent mainstream integrated platforms and are significant directions for the development of IROGs, as shown in Fig. 5(f).

Researchers have proposed doping and dispersion control schemes to improve the optical performance of optical microcavities[43]. In 2007, Hsiao *et al.*[27] used ion exchange to prepare an active integrated optical ring resonator in neodymium-doped glass, which compensated for transmission losses. The finesse of the 1.6-cm diameter ring resonator increased from 11 to 250. The research team at Beihang University proposed a three-dimensional vertically coupled resonator structure[44], which was directly written on doped phosphate glass using a femtosecond laser. The experimental results showed that when the pump power was 50 mW, the measurement limit precision could reach 5.3 deg/h. The principle of dispersion control is to change the group velocity of the light waves, making them accelerate (slow down) as fast (slow) light. Slow light corresponds to normal dispersion, and fast light corresponds to anomalous dispersion. The commonly used scheme for structural dispersion control is to design a special coupled resonator waveguide (CROW)[43]. This type of gyroscope based on an anomalous dispersion structure is also called a fast light gyroscope.

Beihang University is a major research unit in the field of dispersion control[42–48]. In 2016, Zhang *et al.* of Beihang University proposed using erbium-doped lithium niobate film to prepare a CROW[46], as shown in Fig. 6. The dispersion relationship of the entire CROW was modulated by adjusting the phase of the Mach–Zehnder interferometer (MZI), thereby improving the sensitivity of the IROGs. In 2019, they proposed placing the dispersion medium in a slit resonator and using the linewidth broadening of the resonator to measure the rotation angular velocity of the gyroscope[49]. This self-referenced measurement method does not depend on high-Q microcavities and can eliminate the lock-in effect of the resonant gyroscope. This scheme enhances the sensitivity of the gyroscope by at least four

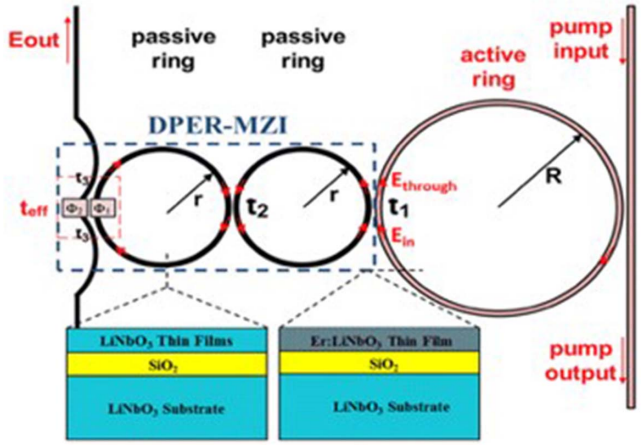

Fig. 6. Schematic diagram of CROW[46].

orders of magnitude in a low Q micro-resonator. In addition to doping and dispersion control, some researchers have also utilized nonlinear effects[50] and weak value amplification[51] to enhance the performance of optical microcavities and achieve high-performance IROGs.

3.2 Sagnac effect enhancement

One method to improve the performance of IROGs is to enhance the Sagnac effect, in addition to increasing the optical performance of the resonant cavity. Various schemes have been proposed to enhance the Sagnac effect, including reducing noise, utilizing Brillouin scattering, exploiting exceptional points, and using exceptional surfaces.

In 2018, researchers from the California Institute of Technology[42] utilized the reciprocity of a passive optical network to increase the gyroscope signal-to-noise ratio, resulting in the development of the world's smallest gyroscope on a 2 mm^2 silicon chip with a random walk angle of 650 deg/$\sqrt{h}$. Notable research groups working on Brillouin scattering include Zhang's and Silver's team at Caltech[49,50], the University of California, Santa Barbara, and Honeywell[51]. Li's team proposed the SiO_2 micro-ring-based Brillouin gyroscopes in 2017[52] and in

2020, Lai *et al.* proposed the chip-scale ring laser gyroscope[53], both demonstrating the ability to measure Earth's rotation due to its stability and sensitivity. The team at the University of California, Santa Barbara collaborated with Honeywell in 2019[54] to develop a low-loss SiN micro-ring-based Brillouin gyroscope that operates in the 405 nm to 2350 nm wavelength range and can be integrated with other optical components. The use of exceptional points has also been explored by several research teams, including the California Institute of Technology[55], Politecnico di Bari[56–58], Pennsylvania State University[59], and Harbin Engineering University[60] [Fig. 7(a)]. The De Carlo group at Politecnico di Bari proposed parity-time (PT) symmetric[56] and anti-parity-time (APT) symmetric[57] optical gyroscopes in 2017 and 2020, respectively. APT symmetric gyroscopes have been shown to exhibit better performance, displaying a real eigenfrequency splitting. Moreover, Zhong *et al.*[61] introduced the concept of an exceptional surface (ES), which is a high-dimensional feature surface embedded with numerous exceptional points. Research groups at Beihang University[62], Tsinghua University[63,64], and Michigan Technological University[61] have made significant progress in studying ES, as shown in Fig. 7(b).

From a macro perspective, precision integration of optical gyroscopes can be achieved through two main approaches: utilizing a high Q resonant cavity and an enhanced Sagnac effect. The sensitivity of the IOGs is inversely proportional to the Q value and cavity length of the resonant cavity. While a longer cavity length leads to higher Q values, it does not meet the requirement for small-sized integration. To address this issue, future development of IOGs will focus on achieving high Q values with shorter cavity lengths, which will require improvements in fabrication processes to reduce optical losses and achieve high-performance IOGs in smaller volumes. Regarding the resonant micro-cavity platform, SiN and SOI platforms have been extensively investigated for high-precision IROGs, with SiN platforms showing high polarization extinction ratios and SOI platforms being the mainstream platform for future IROGs. In terms of enhancing the Sagnac effect, the development of a Brillouin IROG is expected to be the mainstream direction for the next generation of commercial IROGs. Although significant theoretical and experimental work has been conducted on the sensing performance of exceptional points (EPs) and exceptional surfaces, many aspects of these approaches remain unexplored. Furthermore, the issue of whether EPs and ESs can improve the signal-to-noise ratio in IROGs requires further investigation.

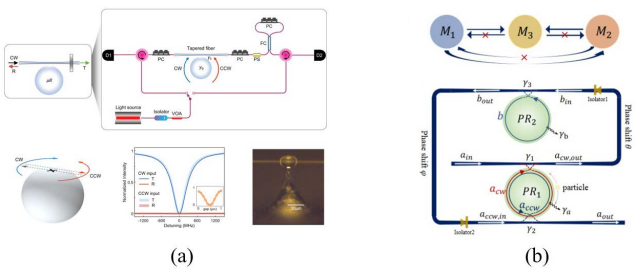

Fig. 7. (a) Schematic diagram of IROGs based on exceptional points[59]. (b) Schematic diagram of IROGs based on exceptional surfaces[63].

4. Conclusion

In this paper, we provide an overview of the research progress in integrated interferometric optical gyroscopes (IIOGs) and integrated resonant optical gyroscopes (IROGs) and compare their strengths and limitations. Our analysis has shown that IIOGs demonstrate superior accuracy, stability, and commercialization potential compared to IROGs.

The fundamental shot noise limited sensitivities[5] of the IIOGs and IROGs can be represented by Eqs. (1) and (2) for ease of comparison,

$$\delta\Omega \approx \frac{\left(\frac{c}{LD}\right)\left(\frac{\lambda_0}{2}\right)}{(\eta_D N_p \tau)^{1/2}}, \tag{1}$$

$$\delta\Omega \approx \frac{\left(\frac{c}{LD}\right)\left(\frac{\lambda_0}{F}\right)}{(\eta_D N_p \tau)^{1/2}}, \tag{2}$$

where $\delta\Omega$ is the uncertainty in the rotation rate caused by the presence of shot noise; c and λ_0 are the speed of light and wavelength in vacuum, respectively; and η_D and N_p are the quantum efficiency of the photodetector and the number of detected photons per second, respectively. for IIOG, L and D are the length and diameter of the coil, respectively. For the IROGs, L and D are the length and diameter of the resonant cavity, respectively. As seen in Eqs. (1) and (2), the sensitivity of an IROG is comparable to the sensitivity of an IFOG that is $F/2$ times larger (where F is the finesse of the resonant cavity, related to Q). For a finesse value of 100, it is theoretically anticipated that the shot noise-limited sensitivity of the resonator will be fifty times higher when compared under identical conditions of coil length, diameter, and optical power. Consequently, the precision of IIOGs surpasses that of the IROGs. Additionally, IROGs encounter significantly more intricate technical challenges, primarily due to its reliance on an exceptionally coherent light source. Moreover, the mitigation of various parasitic effects in IROGs is not as straightforward nor as efficient as in the case of the IIOGs. In the IIOGs, the use of a broadband, low-coherence source serves as an effective solution to these issues.

In the realm of manufacturing technologies, it is evident that IIOGs and IROGs face distinct challenges. For IIOGs, future research is anticipated to concentrate on hybrid integration. This entails addressing various technical issues, such as reducing coupling losses between the components and optical fibers, suppressing relative intensity noise in light sources, and mitigating polarization noise in optical paths. On the other hand, IROGs show great potential for miniaturization, but achieving small cavity lengths with high Q remains a critical challenge. Furthermore, the development of Brillouin IROGs is poised to become the mainstream direction for the next generation

of commercial IROGs. However, enhancing the signal-to-noise ratio and stability in Brillouin IROGs warrants further exploration. Despite the current limitations related to core materials, fabrication processes, and technologies, IROGs continue to be a highly promising avenue for future integrated optical gyroscopes.

In the realm of material platforms, thin-film lithium niobate is regarded as the most promising platform for achieving high precision. However, challenges such as high polarization extinction ratios and low coupling losses need to be effectively addressed. Meanwhile, silicon-based platforms, which are widely adopted for cost-effective and compact IOGs, require further enhancements to ensure stability across diverse environments.

In summary, optical gyroscopes, as conventionally designed, comprise discrete optical components, leading to larger physical dimensions and intricate assembly processes, which in turn pose challenges for cost reduction. Consequently, the foreseeable trajectory unmistakably points toward the development and production of integrated optical gyroscopes (IOGs). These IOGs are characterized by their potential for large-scale, rapid manufacturing, compact form factors, cost-effectiveness, and enhanced reliability. By elucidating the existing challenges and delineating the prospective research directions for both integrated interferometric optical gyroscopes (IIOGs) and integrated resonant optical gyroscopes (IROGs), our objective is to furnish a comprehensive overview of the current state of this field.

References

1. F. Bi, D. Zhang, L. Lu, *et al.*, "Latest progress of integrated optical gyroscopes sensitive unit," Laser Optoelectron. Prog. **58**, 0700005 (2021).
2. H. Arianfard, S. Juodkazis, D. J. Moss, *et al.*, "Sagnac interference in integrated photonics," Appl. Phys. Rev. **10**, 011309 (2023).
3. H.-F. Liu, H.-J. Guo, M.-Q. Tan, *et al.*, "Research progress of lithium niobate thin film modulators," Chin. Opt. **15**, 1 (2022).
4. J. Geng, L. Yang, S. Zhao, *et al.*, "Recent development of resonant micro cavity in resonant micro-optical gyro," Infrared Laser Eng. **50**, 20210044 (2021).
5. H. C. Lefevre, *The Fiber-Optic Gyroscope*, 3rd ed. (Artech House, 2022).
6. M. Sorel and P. J. R. Laybourn, "Progress on the GaAlAs Ring Laser Gyroscope," Alt Freq. **10**, 45 (1998).
7. S. Donati, *Electro-Optical Instrumentation: Sensing and Measuring with Lasers* (Pearson Education, 2004).
8. L. Wang, D. R. Halstead, T. D. Monte, *et al.*, "Low-cost, high-end tactical-grade fiber optic gyroscope based on photonic integrated circuit," in *IEEE International Symposium on Inertial Sensors and Systems (INERTIAL)* (2019), p. 1.
9. K. Shang, M. Lei, Q. Xiang, *et al.*, "Near-navigation-grade interferometric fiber optic gyroscope with an integrated optical chip," Chin. Opt. Lett. **18**, 120601 (2020).
10. X. Suo, H. Yu, and X. Wu, "Integrated interferometric fiber optic gyroscope employing a photo-electronic chip," IEEE Photon. Technol. Lett. **34**, 1250 (2022).
11. A. Rickman, "The commercialization of silicon photonics," Nat. Photonics **8**, 579 (2014).
12. M. A. Tran, T. Komljenovic, J. C. Hulme, *et al.*, "Integrated optical driver for interferometric optical gyroscopes," Opt. Express **25**, 3826 (2017).
13. Y.-C. Wang, S.-Y. Lu, M.-C. Chan, *et al.*, "CMOS-enabled silicon photonics driver chip for interferometric fiber optics gyroscope," in *IEEE International Symposium on Inertial Sensors and Systems (INERTIAL)* (2022), p. 1.
14. X. Yi and X. Wen, "Y-integrated optic chip (Y-IOC) applied in fiber optic gyro," Proc. SPIE **6344**, 63440U (2006).
15. O. Deppe, G. Dorner, S. König, *et al.*, "MEMS and FOG technologies for tactical and navigation grade inertial sensors—recent improvements and comparison," Sensors **17**, 567 (2017).
16. J. Liu, C. Zhang, F. Gao, *et al.*, "Method for improving the polarization extinction ratio of multifunction integrated optic circuits," Opt. Express **29**, 28096 (2021).
17. H. Guo, H. Liu, Z. Wang, *et al.*, "Design of a novel Y-junction electro-optic modulator based on thin film lithium niobite," J. Infrared Millim. Waves **41**, 279 (2022).
18. K. Shang, M. Lei, Q. Xiang, *et al.*, "Tactical-grade interferometric fiber optic gyroscope based on an integrated optical chip," Opt. Commun. **485**, 126729 (2021).
19. C.-G. Li, J.-Y. Yang, X.-H. Li, *et al.*, "Design and fabrication of the GaAs integrated optical chip for fiber optical gyroscope," Optoelectron. Lett. **6**, 269 (2010).
20. S. Stopiński, A. Jusza, and R. Piramidowicz, "An interferometric fiber-optic gyroscope system based on an application specific photonic integrated circuit," in *European Conference on Lasers and Electro-Optics and European Quantum Electronics Conference* (2017), paper CH_7_1.
21. B. Wu, Y. Yu, and X. Zhang, "Mode-assisted silicon integrated interferometric optical gyroscope," Sci. Rep. **9**, 12946 (2019).
22. D. Liu, H. Li, X. Wang, *et al.*, "Interferometric optical gyroscope based on an integrated silica waveguide coil with low loss," Opt. Express **28**, 15718 (2020).
23. S. Srinivasan, R. Moreira, D. Blumenthal, *et al.*, "Design of integrated hybrid silicon waveguide optical gyroscope," Opt. Express **22**, 24988 (2014).
24. S. Gundavarapu, M. Belt, T. A. Huffman, *et al.*, "Interferometric optical gyroscope based on an integrated Si_3N_4 low-loss waveguide coil," J. Lightwave Technol. **36**, 1185 (2018).
25. B. Wu, Y. Yu, J. Xiong, *et al.*, "Silicon integrated interferometric optical gyroscope," Sci. Rep. **8**, 8766 (2018).
26. P. Del'Haye, S. A. Diddams, and S. B. Papp, "Laser-machined ultra-high-*Q* microrod resonators for nonlinear optics," Appl. Phys. Lett. **102**, 221119 (2013).
27. H.-K. Hsiao and K. A. Winick, "Planar glass waveguide ring resonators with gain," Opt. Express **15**, 17783 (2007).
28. H.-Y. Yu, C.-X. Zhang, L.-S. Feng, *et al.*, "SiO_2 waveguide resonator used in an integrated optical gyroscope," Chin. Phys. Lett. **26**, 054210 (2009).
29. L. Ning, L. Guo, M. Kong, *et al.*, "Waveguide-type optical passive ring resonator gyro using frequency modulation spectroscopy technique," J. Semicond. **35**, 124008 (2014).
30. J. Zhang, H. Ma, H. Li, *et al.*, "Single-polarization fiber-pigtailed high-finesse silica waveguide ring resonator for a resonant micro-optic gyroscope," Opt. Lett. **42**, 3658 (2017).
31. C. Feng, Y. Zhang, H. Ma, *et al.*, "Improving long-term temperature bias stability of an integrated optical gyroscope employing a Si_3N_4 resonator," Photonics Res. **10**, 1661 (2022).
32. C. Feng, D. Zhang, Y. Zhang, *et al.*, "Resonant integrated optical gyroscope based on Si_3N_4 waveguide ring resonator," Opt. Express **29**, 43875 (2021).
33. Y. M. He, F. H. Yang, W. Yan, *et al.*, "Asymmetry analysis of the resonance curve in resonant integrated optical gyroscopes," Sensors **19**, 3305 (2019).
34. X.-M. Xue, J. Tang, H.-L. Zhou, *et al.*, "All-polymer monolithic resonant integrated optical gyroscope," Opt. Express **30**, 42728 (2022).
35. T. Zhang, G. Qian, Y.-Y. Wang, *et al.*, "Integrated optical gyroscope using active Long-range surface plasmon-polariton waveguide resonator," Sci. Rep. **4**, 3855 (2014).
36. C. Ciminelli, F. Dell'Olio, M. N. Armenise, *et al.*, "High performance InP ring resonator for new generation monolithically integrated optical gyroscopes," Opt. Express **21**, 556 (2013).
37. A. A. Savchenkov, A. B. Matsko, V. S. Ilchenko, *et al.*, "Optical resonators with ten million finesse," Opt. Express **15**, 6768 (2007).
38. W. Liang, V. S. Ilchenko, A. A. Savchenkov, *et al.*, "Resonant microphotonic gyroscope," Optica **4**, 114 (2017).
39. A. Biberman, M. J. Shaw, E. Timurdogan, *et al.*, "Ultralow-loss silicon ring resonators," Opt. Lett. **37**, 4236 (2012).
40. G. Qian, T. Zhang, L.-J. Zhang, *et al.*, "Demonstrations of centimeter-scale polymer resonator for resonant integrated optical gyroscope," Sens. Actuators A **237**, 29 (2016).

41. Y.-Y. Wang and T. Zhang, "Spontaneous emission noise in long-range surface plasmon polariton waveguide based optical gyroscope," Sci. Rep. **4**, 6369 (2014).
42. P. P. Khial, A. D. White, and A. Hajimiri, "Nanophotonic optical gyroscope with reciprocal sensitivity enhancement," Nat. Photonics **12**, 671 (2018).
43. M. Mohammadi, S. Olyaee, and M. Seifouri, "Design and optimization of passive optical gyroscope, based on nanostructures ring resonators for rotation sensing applications," Opt. Quantum Electron. **54**, 696 (2022).
44. J. Chen, H. Zhang, J. Jin, *et al.*, "Optimization of gyroscope properties with active coupled resonator optical waveguide structures," Proc. SPIE **9378**, 93781Q (2015).
45. H. Zhang, W. Li, P. Han, *et al.*, "The effect of broadened linewidth induced by dispersion on the performance of resonant optical gyroscope," Opt. Commun. **407**, 208 (2018).
46. H. Zhang, J. Liu, J. Lin, *et al.*, "On-chip tunable dispersion in a ring laser gyroscope for enhanced rotation sensing," Appl. Phys. A **122**, 501 (2016).
47. X. Chang, H. Zhang, W. Li, *et al.*, "Sensitivity enhancement of a dispersive cavity with squeezed vacuum light injection," J. Opt. Soc. Am. B **39**, 1815 (2022).
48. J. Lin, J. Liu, H. Zhang, *et al.*, "Theoretical analyses of resonant frequency shift in anomalous dispersion enhanced resonant optical gyroscopes," Sci. Rep. **6**, 38759 (2016).
49. H. Zhang, W. Li, P. Han, *et al.*, "Mode broadening induced by rotation rate in an atom assisted microresonator," J. Appl. Phys. **125**, 084502 (2019).
50. J. M. Silver, L. Del Bino, M. T. M. Woodley, *et al.*, "Nonlinear enhanced microresonator gyroscope," Optica **8**, 1219 (2021).
51. M. Song, J. Nauriyal, J. Steinmetz, *et al.*, "Integrated optical gyroscope with inverse weak value amplification," in *Conference on Lasers and Electro-Optics (CLEO)* (Optica Publishing Group, 2022), p. 1.
52. J. Li, M.-G. Suh, and K. Vahala, "Microresonator Brillouin gyroscope," Optica **4**, 346 (2017).
53. Y.-H. Lai, M.-G. Suh, Y.-K. Lu, *et al.*, "Earth rotation measured by a chip-scale ring laser gyroscope," Nat. Photonics **14**, 345 (2020).
54. S. Gundavarapu, G. M. Brodnik, M. Puckett, *et al.*, "Sub-hertz fundamental linewidth photonic integrated Brillouin laser," Nat. Photonics **13**, 60 (2019).
55. Y.-H. Lai, Y.-K. Lu, M.-G. Suh, *et al.*, "Observation of the exceptional-point-enhanced Sagnac effect," Nature **576**, 65 (2019).
56. M. De Carlo, F. De Leonardis, and V. M. N. Passaro, "Design rules of a microscale PT-symmetric optical gyroscope using group IV platform," J. Lightwave Technol. **36**, 3261 (2018).
57. M. De Carlo, F. De Leonardis, L. Lamberti, *et al.*, "High-sensitivity real-splitting anti-PT-symmetric microscale optical gyroscope," Opt. Lett. **44**, 3956 (2019).
58. M. De Carlo, F. De Leonardis, L. Lamberti, *et al.*, "Design of a resonator-bus-resonator anti-parity-time-symmetric integrated optical gyroscope," Opt. Lasers Eng. **153**, 106983 (2022).
59. S. Soleymani, Q. Zhong, M. Mokim, *et al.*, "Chiral and degenerate perfect absorption on exceptional surfaces," Nat. Commun. **13**, 599 (2022).
60. Y. Zhang, J. Geng, L. Li, *et al.*, "Exceptional-point-enhanced Brillouin micro-optical gyroscope based on self-injection locking," Opt. Commun. **528**, 129008 (2023).
61. Q. Zhong, J. Ren, M. Khajavikhan, *et al.*, "Sensing with exceptional surfaces in order to combine sensitivity with robustness," Phys. Rev. Lett. **122**, 153902 (2019).
62. W. Li, Y. Zhou, P. Han, *et al.*, "Exceptional-surface-enhanced rotation sensing with robustness in a whispering-gallery-mode microresonator," Phys. Rev. A **104**, 033505 (2021).
63. H. Yang, X. Mao, G.-Q. Qin, *et al.*, "Scalable higher-order exceptional surface with passive resonators," Opt. Lett. **46**, 4025 (2021).
64. G.-Q. Qin, R.-R. Xie, H. Zhang, *et al.*, "Experimental realization of sensitivity enhancement and suppression with exceptional surfaces," Laser Photonics Rev. **15**, 2000569 (2021).